Combining Transition Metals – An Approach towards High-Performing Coking Tolerant Solid Oxide Fuel Cell Anodes

Drasbæk, D. B.; Traulsen, M. L.; Sudireddy, B. R.; Holtappels, P.

Published in:
ECS Transactions

Link to article, DOI:
10.1149/09101.1953ecst

Publication date:
2019

Document Version
Peer reviewed version

Combining Transition Metals – An approach towards High-performing Coking Tolerant Solid Oxide Fuel Cell Anodes

D. B. Drasbæk[a], M. L. Traulsen[a], B. R. Sudireddy[a], and P. Holtappels[a]

[a] Department of Energy Conversion and Storage, Technical University of Denmark, Denmark

Bimetallic combinations of the three transition metals, Ni, Co, and Fe, were infiltrated alongside gadolinium doped ceria (CGO), into a strontium titanate backbone. The infiltrated cells were analyzed using electrochemical impedance spectroscopy in the temperature range 650°-850°C and in the atmospheres: 4% H_2O/H_2, 50% H_2O/H_2, 80% H_2O/H_2, and 50% CO_2/CO. In addition, *in situ* synchronous Raman spectroscopy and EIS experiments were performed to explore the coking tolerance of the bimetallic infiltrations. The electrocatalytic activity of the bimetals were similar to the single metals with electrode area specific resistances 0.35 Ωcm^2, 0.28 Ωcm^2, and 1.32 of Ωcm^2 for the Co-Fe-CGO, Ni-Co-CGO, and Ni-Fe-CGO infiltrated cells, respectively, at 750ºC in 50% H_2O/H_2. The results obtained from the synchronous *in situ* Raman - EIS experiments further indicates an improved coking resistance for combined transition metal infiltrations.

Introduction

Ni/YSZ cermet electrodes are state of the art and are effective for the oxidation of H_2, but suffer from degradation in performance when exposed to redox cycling and when poisoned by impurities such as sulphur in the fuel (1). Furthermore, these state of the art Ni/YSZ anodes are susceptible to carbon deposition when operated with carbon containing fuels and finally they suffer from loss of nickel percolation over time, which causes a detrimental loss of conductivity within the electrode (2).

For several decades, research efforts have been directed towards the improvement of the SOFC anode materials. One strategy to overcome some of the challenges with the Ni/YSZ anodes is to decouple the electrode functionalities, by separating the electronically conductive phase from the electrocatalytic phase. This would enable design of a backbone material which is both redox stable and which has the desired electrical conductivity.

One possible backbone material is the Nb-doped strontium titanate (STN), which is known to be highly redox stable, tolerant to oxygen, carbon, and sulphur containing atmospheres and to have a suitable electronic conductivity. However, the STN based SOFC anodes suffer from a too low ionic conductivity (3), (4), for which reason ionic conductivity must be introduced in order to extend the triple phase boundary into the electrode structure.

In previous work performed by Drasbæk et. al. it was found that nickel, cobalt, and iron nanoparticles each have some desirable properties, depending on the fuel atmosphere. In short, it was found that the nickel and cobalt infiltrated STN94 anodes have similar performance in all atmospheres, while the iron infiltrated samples was found to be too unstable in performance with changes in the pO_2 (to be published). Furthermore, *in situ* synchronous Raman spectroscopy and EIS coking studies of the nickel and cobalt

infiltrated STN94 have indicated that the cobalt infiltration experience insignificant carbon deposition when exposed to pure methane at 850ºC, while the nickel infiltrated STN94 cells experiences carbon deposition (5).

The scope of this work is hence to explore if combinations of two transition metals together with CGO, can lead to an improved stability and coking resistance when infiltrated into STN94 based anodes. This is done by characterizing both the combinations of two metals with CGO, but also by investigating the individual metals infiltrated with CGO. The investigation of the performance and stability is done by using electrochemical impedance spectroscopy (EIS) in the temperature range 650-850ºC in the atmospheres: 4% H_2O/H_2, 50% H_2O/H_2, 80% H_2O/H_2, and 50% CO_2/CO. In addition, the coking resistance of the cells are evaluated using *in situ* synchronous Raman spectroscopy and EIS, which makes it possible to compare changes in the surface chemistry to changes in the impedance response.

Experimental

Cell fabrication and infiltration for electrochemical characterization

The electrochemical characterization was performed using symmetrical cells. These cells were fabricated using spray deposition, where the $Sr_{0.94}Ti_{0.9}Nb_{0.1}O_3$ (STN94) ink was spray deposited on both sides of a pre-sintered 230-250 μm thick Sc_2O_3, Y_2O_3 co-stabilized ZrO_2 (ScYSZ) electrolyte and sintered at 1200 ºC, for 8 hours in air. The sintered electrode thickness ranged between 10 and 20 μm. After sintering, the cells were laser cut into 0.6 cm × 0.6 cm dimensions to perform electrochemical testing. The infiltration solutions were prepared by making an aqueous 3M $Ce_{0.8}Gd_{0.20}O$ (CGO) solution, using the respective Ce and Gd nitrates. Thereafter, metal nitrates (Co / Ni / Fe) or combinations of metals (Ni-Co / Ni-Fe / Co-Fe) corresponding to 10 wt.% of CGO, were dissolved in the CGO solution. In addition, a 5 vol.% surfactant was also added to the infiltration solutions. Prior to the infiltration procedure, the symmetrical cells were weighed and the infiltration was then performed using the infiltration procedure described in previous work (5). After the infiltration procedure, the cells were weighed again in order to calculate the infiltration load. The average weight gain was 0.80 $mg \cdot cm^{-2}$ for the Ni-CGO, 0.86 $mg \cdot cm^{-2}$ for the Co-CGO, 0.76 $mg \cdot cm^{-2}$ for the Fe-CGO, 0.90 $mg \cdot cm^{-2}$ for the Ni-Co-CGO, 1.36 $mg \cdot cm^{-2}$ for the Ni-Fe-CGO, and 1.21 $mg \cdot cm^{-2}$ for the Co-Fe-CGO infiltrated cells, relative to the total mass of the cells.

Cell Preparation for *In Situ* Synchronous Raman Spectroscopy and EIS

The cells used for the *in situ* synchronous Raman and EIS experiments are identical to the ones described above, except from one point: Prior to the infiltration procedure, they were polished on one edge, thereby making it possible to investigate the interface between the electrode and the electrolyte directly in the Raman microscope. Except from that, the infiltration procedure was performed in a similar way as described above.

Before the *in situ* Raman experiment, a layer of platinum paste was painted onto each electrode to act as current collecting layer, and platinum wires were attached in order to connect to the external circuit. This way of attaching the wires is not ideal and might lead to asymmetric electrical field lines, which may explain why the overall

electrochemical performance observed during these experiments were lower than during the conventional electrochemical characterization experiments.

Structural Characterization

Characterization of sample microstructure before and after testing was carried out using scanning electron microscopy (SEM) (ZEISS Merlin, Carl Zeiss, Germany). The microstructure of the cells was investigated on a fractured cross-section. Furthermore, energy dispersive x-ray spectroscopy (EDS) mapping was performed in order to map the particle composition. Notably, 20 nm thick carbon layer was deposited in order to avoid charging effects.

Electrochemical Characterization

Prior to the electrochemical characterization, a current collecting layer of platinum paste was hand-painted onto the cells. The cells were afterwards mounted in a test house that allows for the simultaneous measurement of four symmetrical cells.

All tested samples were exposed to the same test protocol. However, additionally, some cells were exposed to a 300 hours stability test at the end of the experiment. The test protocol performed on each cell includes testing in 4% H_2O/H_2, 50% H_2O/H_2, 80% H_2O/H_2, and 50% CO_2/CO at different temperatures.

The electrochemical impedance spectroscopy was performed at OCV using a Gamry Reference 600 potentiostat. Impedance spectra were recorded in the frequency range between 0.01Hz-1.0 MHz with 10 points/decade applying a 50 mV amplitude.

In Situ Synchronous Raman Spectroscopy and EIS

The in situ Raman data were obtained using a Renishaw InVia Raman spectrometer system coupled with a Linkam heat-stage, which gives control over the temperature and the gas-composition. The laser used in the experiments was a 532 nm diode laser with a ~1μm diameter beam spot on the sample and a laser power less than 8 mW. The Stokes scattered Raman light from the sample was collected and dispersed onto a CCD detector.

Throughout the *in situ* Raman experiments, electrochemical measurements were performed using a Gamry Reference 600 potentiostat. the time-resolved EIS data were acquired under open circuit potential, with a 25 mV amplitude, between 0.5 Hz-1.0 MHz, with 10 points/decade. During the time-resolved Raman experiments, spectra were acquired continuously with a 30 seconds exposure time per spectrum. Raman data were analyzed in accordance to previous experiments (5).

Through the experiments, the cells were exposed to synthetic air (20% O_2 and 80% N_2), humidified hydrogen (4% H_2O/H_2), 50% CO_2/CO, and 100% CH_4, all with a total gas flow of 1.8 L hr^{-1} at ambient pressure. After each experimental test atmosphere, reference measurements were performed in humidified hydrogen in order to confirm continued cell performance and identify if any degradation had taken place. After the entire experiment the cells were exposed to a re-oxidation, in synthetic air, for comparison with the original surface chemistry. The cell was afterwards cooled to room temperature for *ex situ* analysis.

Results and Discussion

Structural Characterization

The pure STN backbone material can be observed in Figure 1a, in Figure 1b the microstructure of a Ni-Co-CGO infiltrated cells right after the wet infiltration procedure. It is difficult to distinguish the CGO nanoparticles from the metal nanoparticles in image, however, clear indications of infiltration when compared to Figure 1a. Figure 1c shows the surface morphology after the cell has been tested. It is here possible to distinguish the infiltrated CGO from the metal nanoparticles, since the CGO makes a surface that looks like a sponge, while the nanoparticles agglomerates into larger nanoparticles of 50-100 nm in diameter. Finally, EDS mapping of a Ni-Co-CGO infiltrated sample, exposed to the electrochemical test procedure, can be seen in Figure 1d. The EDS show that the spherical particles are neither pure nickel nor pure cobalt, but rather a combination of the two. Unfortunately, it is not possible to make a quantitative analysis of the nickel-cobalt ratio in these nanoparticles, using the EDS data, due to the large probing volume.

The morphology of the infiltrated materials are not identical right after the infiltration procedure. However, it was observed that the final morphology after the electrochemical test-procedure were identical for all tested cells infiltrated with either one metal and CGO or two metals and CGO. This eventually indicates a common morphology during the electrochemical testing.

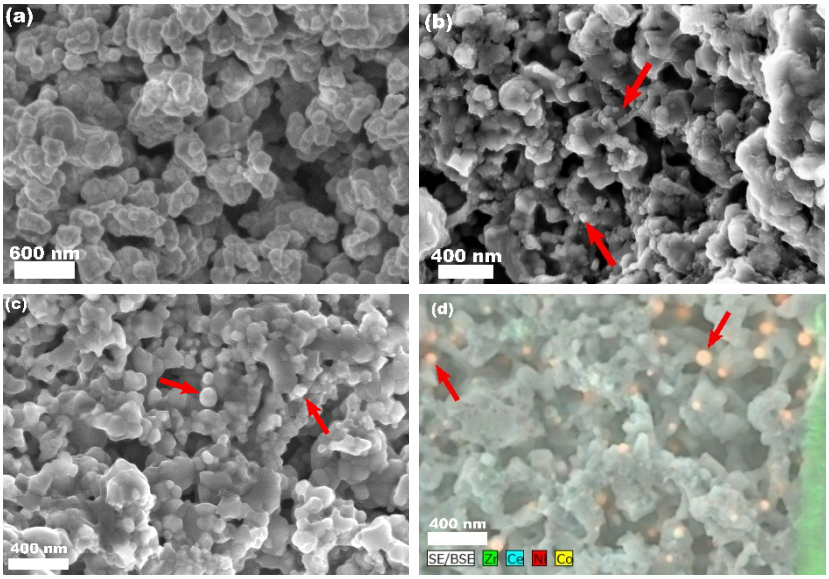

Figure 1. Scanning electron microscopy analysis of a) the pure STN backbone, and Ni-Co-CGO infiltrated cells b) right after calcination, c) after heating to operation temperature (850ºC), and d) EDS mapping of a cell after operation. Examples of the nanoparticles are marked with arrows.

Electrochemical Performance

The characteristic impedance spectra of Co-Fe-CGO, Ni-Co-CGO, and Ni-Fe-CGO infiltrated STN backbones at 750°C in 50% H_2O/H_2 are shown in Figure 2. The impedance spectra indicate an asymmetric shape, and thus more complex models then a single RQ element are required to analyzed the spectra further as regards number and nature of the underlying physical processes. In this paper, emphasis is paid to the total area specific electrode resistance. Thus, the equivalent circuit model used for the fitting of impedance spectra, by the complex-non-linear-least squares method, is L-R-R_1Q_1-R_2Q_2-R_3Q_3 (where Q is a constant phase element, R is the resistance and L is the inductance). An equivalent circuit was used for parameterization of the spectra to derive the ohmic and the electrode area specific resistance (ASR), the sum of R_1, R_2 and R_3, without any further analysis of the underlying reaction mechanism. Examples of this fitting are also shown in Figure 2. The ASR, is the resistance arising from the voltage loss related to the faradaic current in the electrode.

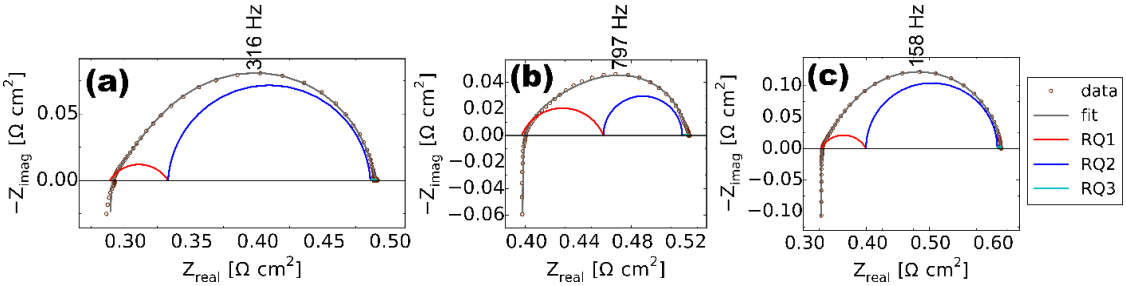

Figure 2. Fitting of the equivalent circuit L-R-RQ-RQ-RQ, for a) a Co-Fe-CGO symmetrical cell, b) a Ni-Co-CGO symmetrical cell, and c) a Ni-Fe-CGO symmetrical cell in 50% H_2O/H_2 at 750°C.

Figure 3 gives an overview of the total ASRs in 4% H_2O/H_2 and 50% H_2O/H_2 at 750°C. It can be observed in Figure 3 that the iron containing cells have higher ASRs, both when iron is present as a single metal and as a bi-metal. This indicates that iron has a detrimental influence on the ASRs. Furthermore, it can be observed in Figure 3a, that the Ni-CGO and Co-CGO infiltrated cells have averaged ASRs of 0.22±0.02 and 0.27±0.08 Ω·cm2. When these values are compared with the averaged ASR of the Ni-Co-CGO, which is 0.30±0.06 Ω·cm2, it is clear that combining the nickel and the cobalt does not improve the performance in regards to the ASR. The same trend is observed in Figure 3b, since the ASR of the Ni-CGO, the Co-CGO, and the Ni-Co-CGO infiltrated cells are 0.29±0.05, 0.44±0.15, and 0.28±0.14 Ω·cm^2, respectively. Notably, the total ASR for the pure STN backbone is 117.3±32.0 and 91.2±16.5 in 4% H_2O/H_2 and 50% H_2O/H_2.

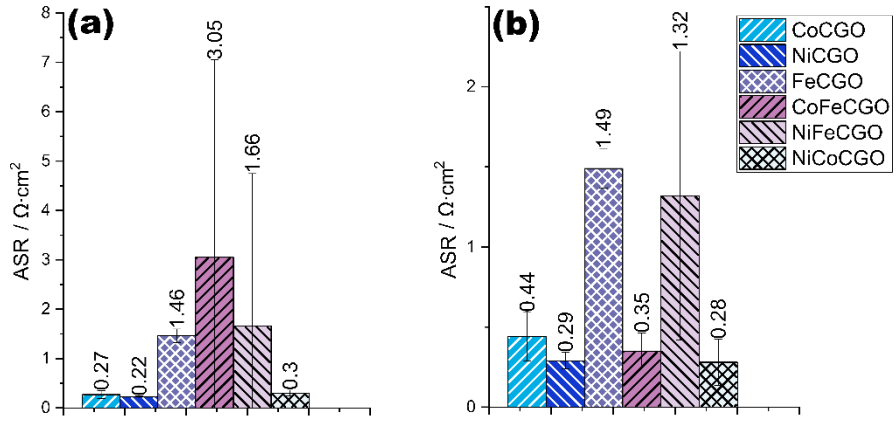

Figure 3. Averaged total ASR of the different infiltrations, in a) 4% H_2O/H_2 at 750ºC and in b) 50% H_2O/H_2 at 750ºC.

One approach to gain further insight into the overall influence of the infiltrations on the electrochemical reaction mechanism is to look at the temperature dependence of the ASRs. It was found that the ASR for all infiltrated cells show an Arrhenius behavior in the investigated temperature range. The averaged activation energy was estimated from the Arrhenius equation and can be seen in Figure 4. Since the activation energy with Ni an Co infiltrated as single metals is similar to the activation energy when the metals are infiltrated as bimetals, it indicates that no change in reaction mechanism is occurring from single metals to bi-metals. In contrast, bimetallic infiltrations including Fe show an activation energy similar to the activations energies achieved for Ni and Co infiltration. This indicates that the latter two metals dominate the reaction mechanisms in bimetals including Fe.

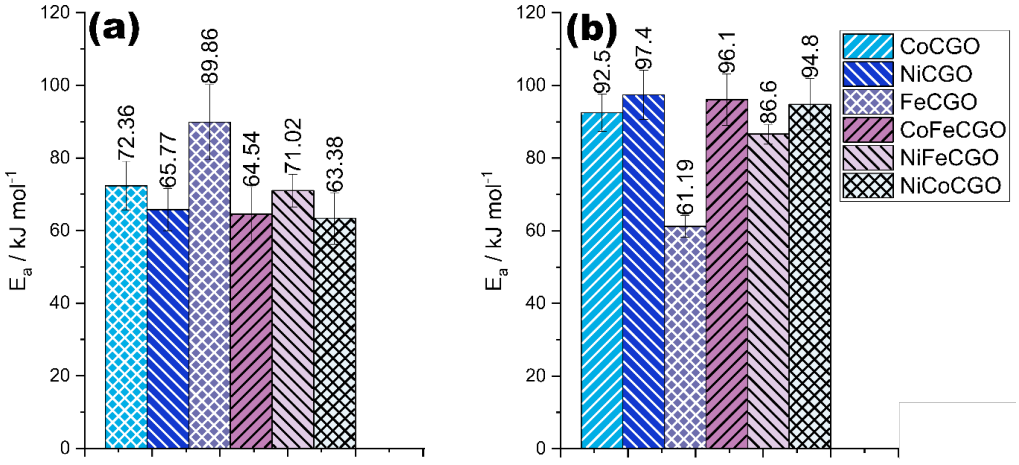

Figure 4. The averaged activation energy measured in kJ·mol^{-1} in a) 4% H_2O/H_2 and in b) 50% H_2O/H_2. Notably, the metal catalyst loading of the pure metal infiltrated cells, are 10 times higher than the cells, which have been co-infiltrated with CGO.

It is a known from previously published work, and from the microstructural characterization seen in Figure 1, that the nanoparticles agglomerates into larger spherical particles at operational temperatures (6). Hence, it is of interest to perform a 300 hours stability test at 650ºC in 50% H_2O/H_2 under OCV conditions, of the Ni-Co-CGO, Ni-Fe-CGO and Co-Fe-CGO infiltrated cells. An impedance spectra were measured on each cell every fourth hour, in order to estimate the continuous degradation observed on the cell.

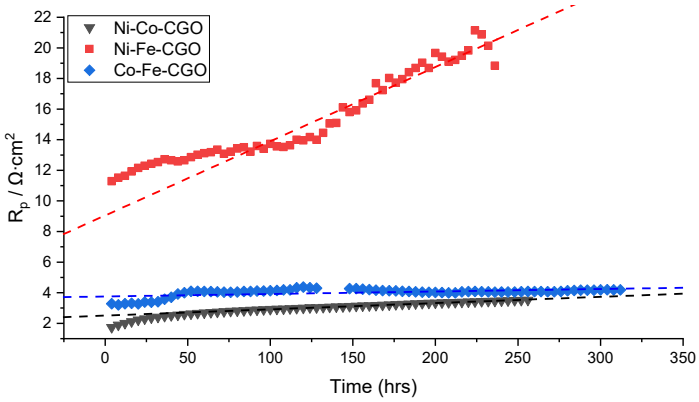

Figure 5: The total ASR as a function of time for a Ni-Co-CGO, a Ni-Fe-CGO and a Co-Fe-CGO infiltrated cell in 50% H_2O/H_2 at 650 ºC

The degradation in cell performance is faster for the Ni-Fe-CGO infiltrated cells, when compared to the Co-Fe-CGO and Ni-Co-CGO infiltrated cells (Figure 5), and degradation rates of 1.63, 4.08, and 48.48 $\Omega \cdot cm^2 \cdot khr^{-1}$ for the Co-Fe-CGO, Ni-Co-CGO, and Ni-Fe-CGO infiltrated cells are achieved.

Coking Tolerance - *In Situ* Synchronous Raman Spectroscopy and EIS

It is known, from previous studies, that the nickel infiltrated STN cells experiences coking when exposed to dry methane, at 850ºC (5). On the other hand, the cobalt infiltrated cell does not experience any coking under the same condition (5). *In situ* synchronous Raman spectroscopy and EIS studies was therefore performed on Ni-CGO and Ni-Co-CGO infiltrated samples.

When carbon accumulates onto the anode surface, carbon deposits will take the form of well-known graphitic carbon (7). These structures give rise to two specific Raman signals, commonly known as the G-band (at 1580 cm^{-1}) and the D-band (at 1350 cm^{-1}). Furthermore, at elevated temperatures, Raman features are expected to shift towards lower energies due to the thermally induced lattice expansion (8).

The Raman data obtained from the Ni-CGO infiltrated cells during the exposure to pure methane at 750ºC, can be seen in Figure 6a. In the Raman spectra, time 0 indicates the moment at which the gas was switched from humidified hydrogen to pure methane. It can in Figure 6a be seen that there is no continuous buildup of carbon in the electrode, however, the G-band peak does show up during the first part of the methane exposure, but is removed again. This is also visible in Figure 6b, were the intensity of the G-band is plotted against time, together with the total ASR measured in the cell. It can be seen in Figure 6b that the rise in the intensity of the G-band occurs simultaneously with a rise in ASR. However, large variations is observed in both the G-band intensity and the ASR during the methane exposure, which are yet to be fully understood, but suggests a temperature change since a similar trend in the serial resistance was observed.

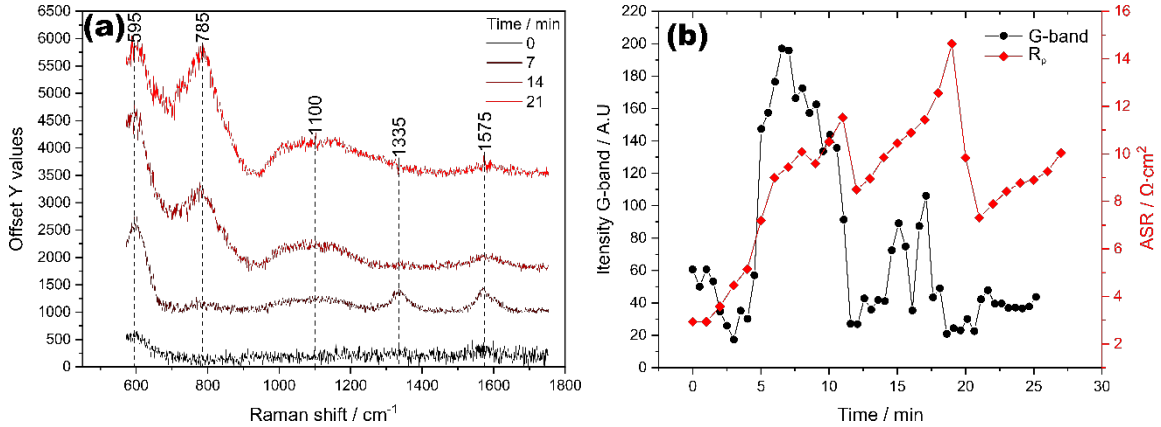

Figure 6. a) Raman spectra of the Ni-CGO infiltrated cells, when exposed to CH_4, please notice that the spectra are vertically shifted for clarity and the broad peak observed around 785 cm^{-1} originates from the STN electrode material. b) The peak intensity of the G-band plotted together with the total ASR of the Ni-CGO infiltrated cell as a function of time.

The Raman data obtained from the Ni-Co-CGO infiltrated cell is observed in Figure 7a. No deposition of carbon can be observed during the methane exposure for this type of cell, however, the total ASR of the cell increases linearly within the first 10 minutes. The ASR, then suddenly drops by a factor three within one minute and thereafter remains more or less constant. The linear increase in the ASR of the Ni-Co-CGO infiltrated cell at the beginning of the methane exposure has yet to be understood and motivates further investigation. It can in Figure 7b be observed that the intensity of the G-band remains constant and the fluctuations can be attributed to noise in the spectra. Hence, it is clear that, the amount of deposited carbon is lower on these cells, when compared to the Ni-CGO infiltrated cell. This suggests that infiltrating a combination of cobalt, nickel, and CGO together, gives a higher degree of coking resistance when compared to the Ni-CGO infiltrated cells. This increase in coking resistance is hence, attributed to the presence of cobalt.

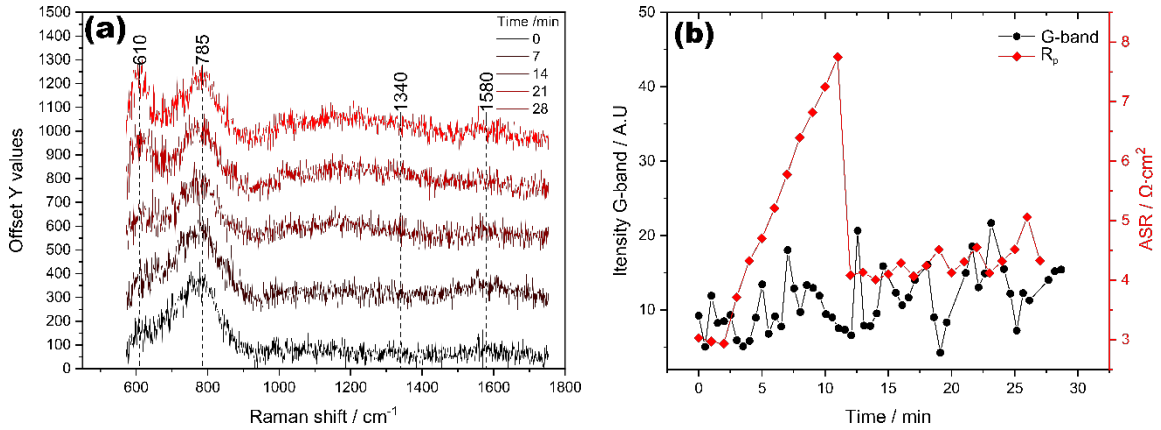

Figure 7. a) Raman spectra of the Ni-Co-CGO infiltrated cells, when exposed to CH_4, please notice that the spectra are vertically shifted for clarity and the broad peak observed around 785 cm^{-1} originates from the STN electrode material. b) The peak intensity of the G-band plotted together with the total ASR of the Ni-Co-CGO infiltrated cell as a function of time.

Conclusion

In this work, bimetallic combinations of nickel, cobalt and iron, infiltrated together with CGO, have been investigated as electrocatalyst for anodes in solid oxide fuel cells. A comparison has been made to the performance achieved with the same metals infiltrated as monometals in a similar manner. Co-Ni bimetals infiltrated with CGO showed similar ASR and activation energy to the Co-CGO and Ni-CGO infiltrated cells. On the other hand it was found that when Fe is infiltrated in the combination with Co or Ni, an increase in the ASR is observed compared to the Co-CGO and Ni-CGO infiltrated cells. The stability of the infiltrated cells was investigated and the Co-Fe-CGO and the Ni-Co-CGO infiltrations had degradation rates of 1.63 and 4.08 $\Omega \cdot cm^2 \cdot khr^{-1}$ over the first 300 h in 50% H_2O/H_2 at 650 ºC and OCV conditions.

The *in situ* synchronous Raman-EIS studies were used to investigate the susceptibility of the Ni-CGO and Ni-Co-CGO infiltrated cells to coking when exposed to pure methane at 750ºC. It was found that the Ni-CGO were more prone to coking than the Ni-Co- infiltrated cells, since no coking was taking place in the Ni-Co-CGO infiltrated cells above the detection limit of the Raman spectrometer.

The fact that combining nickel, cobalt, and CGO does not affect neither the ASR, nor the activation energy in any negative way, combined with the appearance of a higher degree of coking resistance when exposed to carbon containing atmospheres, suggest that the Ni-Co-CGO infiltrated cells should be further investigated as anodes for SOFC.

Acknowledgments

The authors acknowledge colleagues at DTU Energy for technical assistance and fruitful discussions. Furthermore, the authors would like to acknowledge the financial support from the project “BALANCE” (European Union’s Horizon 2020 research and innovation program under grant agreement number 731224).

References

1. Niakolas, Dimitros K. *Applied Catalysis A: General*, **486**, 123 (2014)
2. L.V. Saraf, D. R. Baer, A. S. Lea, Z. H. Zhu, J. J. Strohm, S. D. Sitzman, and D. L. King. *Journal of The Electrochemical Society,* **157**, B463 (2010)
3. T. Ramos, C. Bernuy-Lopez, B. R. Sudireddy, J. J. Bentzen, W. Zhang, P. S. Jørgensen, L. T. Kuhn. *ECS Transactions,* **45**, 389 (2012)
4. Peter Blennow, Kent K. Hansen, L. Reine Wallenberg, Mogens Mogensen. *Solid State Ionics,* **180**, 63 *(*2009)
5. D. B. Drasbæk, M. L. Traulsen, R. A. Walker, and P. Holtappels. *Fuel Cells - From Fundamental to Systems.* 2019.
6. J. M. Vohs, and R. J. Gorte. *Advanced Materials.* **21**, 943 (2009)
7. Mildred S. Dresselhaus, Ado Jorio, Mario Hofmann, Gene Dresselhaus, and Riichiro Saito. *Nano letters* **10**, 751 (2010)
8. Nachiket R. Raravikar, Pawel Keblinski, Apparao M. Rao, Mildred S. Dresselhaus, Linda S. Schadler, and Pulickel M. Ajayan. *Physical review B.* **66**, 235424-1 (2002)